Available online at www.sciencedirect.com
SCIENCE DIRECT®
Carbohydrate Research 340 (2005) 863–874
Carbohydrate RESEARCH

The utility of residual dipolar couplings in detecting motion in carbohydrates: application to sucrose

Richard M. Venable,[a] Frank Delaglio,[b] Scott E. Norris[a] and Darón I. Freedberg[a,*]

[a]*Laboratory of Biophysics, Center for Biologics Evaluation and Research, FDA, 1401 Rockville Pike, HFM-419, MD 20852, USA*
[b]*Laboratory of Chemical Physics, National Institute of Diabetes and Digestive and Kidney Disorders, 5 Center Drive, NIH, Bethesda, MD 20892, USA*

Received 2 December 2004; accepted 18 January 2005

Dedicated to Professor David A. Brant

Abstract—The solution structure and dynamics of sucrose are examined using a combination of NMR residual dipolar coupling and molecular mechanics force fields. It is found that the alignment tensors of the individual rings are different, and that fitting 35 measured residual dipolar couplings to structures with specific ϕ, ψ values indicates the presence of three major conformations: ϕ, ψ = (120°, 270°), (45°, 300°) and (90°, 180°). Furthermore, fitting two structures simultaneously to the 35 residual dipolar couplings results in a substantial improvement in the fits. The existence of multiple conformations having similar stabilities is a strong indication of motion, due to the interconversion among these states. Results from four molecular mechanics force fields are in general agreement with the experimental results. However, there are major disagreements between force fields. Because fits of residual dipolar couplings to structures are dependent on the force field used to calculate the structures, multiple force fields were used to interpret NMR data. It is demonstrated that the pucker of the fructofuranosyl ring affects the calculated potential energy surface, and the fit to the residual dipolar couplings data. Previously published ^{13}C nuclear relaxation results suggesting that sucrose is rigid are not inconsistent with the present results when motional timescales are considered.

Keywords: Sucrose; Residual dipolar coupling; Carbohydrate structure; Carbohydrate dynamics; Heteronuclear NMR

1. Introduction

The flexibility of sucrose, a seemingly well-known sugar, is still controversial. While sucrose is often used as a test system or a simple disaccharide model, it is also important in biological processes. For example, when ingested, sucrose must be enzymatically hydrolyzed to glucose and fructose.[1,2] In order to adhere to teeth *Streptococcus mutans* must bind to sucrose, which results in caries.[3] Sucrose is also bound by proteins that transport it across cell membranes so that it can be used as a nutrient.[4] Each of the above biological processes may require sucrose to assume different conformations. Thus, flexibility in sucrose may be directly related to biological activity.

Initial reports of sucrose's solution structure[5] proposed that the glycosidic torsional angles, ϕ and ψ (Fig. 1), are similar to solid-state values.[6] This conclusion was based on a combination of NMR data, molecular mechanics (hard sphere exoanomeric analysis) calculations, and an inferred hydrogen bond which helps keep sucrose in one conformation.[5] Results from X-plor calculations based on a combination of J couplings, NOEs (nuclear Overhauser enhancements) and a limited number of RDCs (residual dipolar couplings) supported this conclusion.[7] Likewise, field- and temperature-dependent ^{13}C nuclear relaxation and heteronuclear NOE measurements reinforced the idea that sucrose is in a single conformation.[8,9]

Other studies showed evidence of internal motion in sucrose. First, solution-state studies failed to find evidence of a persistent hydrogen bond.[10,11] Another study

* Corresponding author. E-mail: freedberg@cber.fda.gov

0008-6215/$ - see front matter © 2005 Elsevier Ltd. All rights reserved.
doi:10.1016/j.carres.2005.01.025

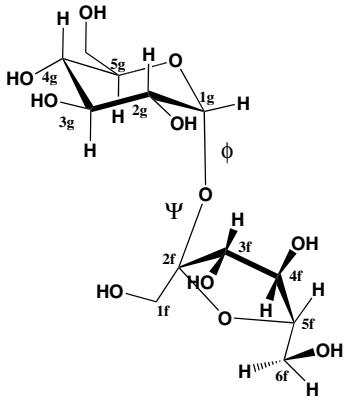

Figure 1. The structure of sucrose defining ϕ and ψ torsions in the disaccharide with numbering scheme used.

yielded temperature- and field-dependent $^{1}H–^{1}H$ NOEs and ROEs (rotating frame Overhauser enhancements) not expected for rigid molecules.[12] A thorough combined NMR and molecular mechanics study of sucrose concluded that the *experimental* observation of two NOE cross-peaks (H-1g to H-4f and H-1g to H-1f) is not consistent with a single structure.[13] Solid-state NMR data on sucrose also supported motion in solution.[14] Finally, an optical rotation study indicated flexibility in sucrose.[15] The flexibility deduced in some of the above studies is based on multiple minima on the PES (potential energy surface). However, it is also possible that the observed flexibility in sucrose arises from librations in a broad shallow minimum.

Flexibility in fructose was deduced from experimental studies.[13,16–18] These studies showed that although fructose is flexible, the pucker is confined to the NE quadrant of the pseudo-rotational wheel, with the phase taking on values between 0° and 90°.

In the presence of liquid-crystalline media, the distribution of molecular orientations is anisotropic, and as a result, dipolar couplings do not sum to zero, as they do under isotropic conditions. The RDCs resulting from partially oriented molecules are straightforward to measure. Over the past few years, studies utilizing RDCs have demonstrated great promise in delineating carbohydrate structure because they provide relative orientations of remote interatomic vectors.[18–22] This type of information is unavailable from *J* couplings or NOEs.[23–25]

Order parameters obtained from fitting RDCs also contain information regarding internal molecular motion.[20,26,27] Molecular tumbling averages otherwise large dipolar couplings to produce high-resolution NMR spectra. All RDCs in a rigid molecule undergoing rapid molecular reorientation are affected in the same way. In contrast, RDCs of rigid fragments making up flexible molecules are averaged according to the motion each fragment experiences and according to rapid molecular reorientation. An example of both types of motion can be found in a recent study of a trisaccharide.[20] In that study,[20] alignment tensors for constituent monosaccharides have similar values when two of the fragments are not moving relative to one another, but take on different values when another fragment is in motion relative to the first two.

Since the structure and dynamics of sucrose have not been fully resolved, we chose to apply RDCs to examine the problem. For each ring, we measured more than the minimum of five independent RDCs required to determine the alignment tensor. Next, we calculated the alignment tensors for the individual rings, which showed that they are moving relative to one another. To investigate the issue of multiple local minima on the PES we fitted single-structure and two-structure models to the RDCs, and observed improved fits for the latter case. These results show strong evidence for internal motion, as they are inconsistent with a single dominant, rigid conformation in sucrose. To aid in interpreting results from RDCs, we consider four published force fields in generating molecular coordinates of sucrose for use in fits to the RDC data. We find that the overall sucrose conformation is influenced by the pucker of the fructofuranosyl ring. We also report that molecular mechanics force fields used to calculate carbohydrate structure can be improved. Finally, we show that results obtained herein do not contradict those obtained by ^{13}C relaxation and X-plor.

2. Materials and methods

Data were collected for two samples at 315 K: (a) a 75 mM sucrose sample in 20 mM phosphate buffer in D_2O at $pD^* = 7.1$; and (b), identical to (a) with added 22% DMPC/DHPC bicelles, as measured from splitting in the ^{2}H signal. DMPC and DHPC, purchased from Avanti Polar Lipids (Alabaster, AL), were used in a molar ratio of 3:1 without further purification. Bicelles were prepared as previously reported[28,29] in 20 mM phosphate buffer in D_2O ($pD^* = 7.1$). The samples were placed in Shigemi microcells (Alison Park, PA), degassed under reduced pressure, and the tops were tightly wrapped with Teflon tape, then Parafilm.

Two-dimensional HSQC and long-range quantitative *J* spectra were taken at a ^{1}H frequency of 500.13 MHz and a ^{13}C frequency of 125.76 MHz on a Bruker Avance 500. Spectra were acquired as previously described,[18] with the exception that INEPT dephasing delays were set to 41.05 ms to collect data for the glucose ring. Two types of long-range correlations were observed in the spectra. In the first, an autocorrelation peak was observed in the corresponding reference spectrum. For these types of peaks, Eq. 1, a variation of a previously published formula,[30] was used to calculate the splittings.

$$J = (2\pi\Delta)^{-1} \times \left(\sin^{-1}\sqrt{\left[V_{\mathrm{lr}}\left(\exp(-t/T_2^{13\mathrm{C}})/\exp(-t/T_2^{12\mathrm{C}})\right)/V_{\mathrm{auto}}(1-\exp(-\tau/T_1))\right]}\right) \quad (1)$$

For long-range correlation peaks which did not show an autocorrelation peak in the reference spectrum, we used those from the long-range, quantitative J spectrum. Splittings were determined according to:

$$J = (2\pi\Delta)^{-1} \times \left(\sin^{-1}\left(\left[\sin(2\pi\Delta^1 J)\right]\sqrt{\left[V_{\mathrm{lr}}\left(\exp(-t/T_2^{13\mathrm{C}})/\exp(-t/T_2^{12\mathrm{C}})\right)/V_{\mathrm{auto}}(1-\exp(-\tau/T_1))\right]}\right)\right) \quad (2)$$

In Eqs. 1 and 2, ^1J is the ^{1}H–^{13}C one-bond splitting measured from HSQC spectra; Δ is the INEPT delay; V_{lr} and V_{auto} are the peak volumes for the correlation peaks and auto-correlation peaks in the long-range spectra, respectively; $\exp(-t/T_2^{13\mathrm{C}})$ is the T_2 decay in cross-peak intensity or volume as a result of the ^{1}H being attached to a ^{13}C in the reference spectrum over the time 4Δ; $\exp(-t/T_2^{12\mathrm{C}})$ is the T_2 decay of cross-peak intensity or volume as a result of ^{1}H's attached to ^{12}C; τ is the recycle delay, and T_1 is the ^{1}H T_1 for a given resonance.[30] $T_2^{13\mathrm{C}}$ and $T_2^{12\mathrm{C}}$ were obtained from a program that calculates ^{1}H relaxation times from the spectral densities using 90 ps as an overall molecular correlation time for sucrose.[31] Eq. 2 corrects a typographical error in the original report.[18]

A fully ^{13}C labeled sucrose sample (Isotec, Miamisburg, OH) provided ^{13}C–^{13}C coupling constants measured from one-dimensional ^{13}C data.[32,33] The ^{1}H–^{1}H coupling constants were measured from COSY spectra taken at 800.13 MHz using ACME.[34] RDCs were calculated from the relation: RDC = $J' - J_{iso}$ where J' and J_{iso} are splittings measured under orienting and isotropic conditions, respectively. We define ${}^n\mathscr{D}_{xy}$ as the n-bond RDC between the nuclei x and y, similar to the convention for J coupling.

2.1. Generation of sucrose conformations

Each structure (molecular geometry with unique ϕ, ψ values) was generated de novo, using internal coordinates for the rings from the crystal structure, minimized in the force field of interest. In this paper, ϕ is the torsional angle defined by the atoms O-5g–C-1g–O-2f–C-2f, and ψ the torsional angle defined by the atoms C-1g–O-2f–C-2f–O-5f (where g and f refer to the glucopyranosyl and fructofuranosyl rings, respectively) (Fig. 1). The ϕ, ψ torsions were set prior to generating Cartesian coordinates, and restrained to the preset values with a force of 400 kcal/mol/rad^2. Torsional sampling was at 5° increments, and included both 0° and 360° as a hysteresis check. Initial calculations were done with the fructose ring unrestrained. In subsequent calculations, the fructose ring pucker phase[35] was restrained to specific values of 0°, 18°, 36°, or 54° using the same force as for the glycosidic torsions.

Each conformation was energy-minimized for 10 steps with a steepest descent algorithm (to relieve bad van der Waals contacts), followed by up to 100 steps using the ABNR (adopted-basis Newton–Raphson) algorithm in CHARMM,[36] with a final 50 steps of full Newton–Raphson minimization. A gradient tolerance of 0.001 was specified for the ABNR algorithm, allowing termination if the gradient was less than the tolerance before completing 100 steps. A non-bond cutoff of 12 Å was employed, using a shifted Lennard–Jones potential and force shifted electrostatics with a constant dielectric of 5.

Finally, it should be noted that only the Accelrys force field[37] provided a residue description for fructose, and the corresponding α anomeric sugar ring linkage found in sucrose. In all cases, it was assumed that glucose parameters were transferable when preparing residue descriptions for fructose.

2.2. Fits of RDCs to structural models

RDCs were fit to structural models using singular value decomposition[38] algorithms available in NMRPipe.[39] Errors in the fits were estimated using a Monte-Carlo subroutine. This was accomplished by adding Gaussian noise to the RDCs and the atomic coordinates, and fitting 100 fictitious data sets. Errors were estimated using a tcl script called dcNoise.tcl, available in NMRPipe.

Multiple conformer averaging was accomplished by using tcl scripts available in NMRPipe. These scripts allowed fitting of more than one set of atomic coordinates, or structures, to the one set of experimentally determined RDCs. Singular value decomposition was then used to find the best two sets of coefficients for the Saupe matrix.

3. Results

3.1. Structure generation and force-field calculations

It is necessary to use molecular mechanics to generate structural models to fit RDCs. In addition to a model, each structure calculation yields an energy value. We

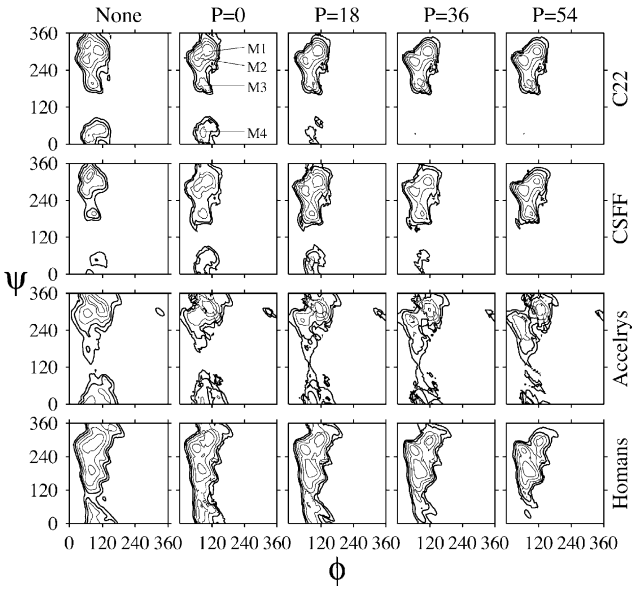

Figure 2. Potential-energy maps displaying relative energies of sucrose structures as calculated with unrestrained (leftmost column) and restrained fructofuranosyl puckers (listed on top of each column) by CHARMM22, CSFF, Accelrys, and Homans force fields (listed on the right side of each row). The contours are drawn at 2 kcal/mol increments relative to the minimum for each map; the bold contours indicate 8 kcal/mol above the minimum. The approximate position of the potential minima are indicated by the labels M1–M4 in the second panel of the top row.

include these maps as they have not previously been compared side-by-side; they reveal subtle differences in force-field parameterization. The surfaces differ more when the pucker is unrestrained, and structures with the same ϕ, ψ values calculated by different force fields yield non-identical χ^2 values. These results illustrate the importance of properly restraining the fructofuranosyl pucker. Energy surfaces generated by the C22 (CHARMM22),[40] CSFF,[41] Homans,[42] and Accelrys[37] force fields in the first column of Figure 2 are the result of restraining only the glycosidic torsions, ϕ and ψ, and yield significantly different PESs, which depend on the force field used. Pucker phases in these structures resulted in geometries, which do not match published experimental data.[13,15–18] To bring the calculated pucker phase values in line with experimental values, sucrose structures were recalculated by simultaneously restraining glycosidic torsions and the pucker phase as described in the Materials and methods section. The energy maps resulting from these calculations show better agreement across force fields, suggesting three regions of ϕ, ψ space as local minima (Fig. 2). These regions will be abbreviated as the ϕ, ψ coordinates are the approximate centers of the respective regions: M1 = (120°, 300°), M2 = (60°, 270°), M3 = (90°, 180°) and M4 = (90°, 40°). Although the ϕ, ψ values of the local minima agree among force fields, their relative energies vary. The energy of M3 is higher than the global minimum and is clearly affected by the pucker phase, as is the shape of the M3 region. However, the general position of M3 does not vary with pucker, remaining at ca. (90°, 180°), while the position of M4 only varies by about 30°. The ϕ, ψ energy maps for C22 and CSFF are fairly consistent, as expected from their common origin; however, they disagree on the stability of M4. Both indicate sampling of M1 and M2, with a barrier between these and the M3 region. The Homans force field implies that M1–M4 are populated, that M3 has a lower energy than C22 and CSFF suggest, and that the barriers to interconversion are low. Finally, the Accelrys force field suggests that M3 is high in energy and a reduced barrier between M4 and the low energy M1 and M2 regions.

3.2. Fits of generated structures to RDCs

To conclusively deduce three-dimensional structure and dynamics it is necessary to measure at least five independent RDCs for each rigid molecular fragment.[38,43,44] Except for C-1g–H-1g, the C–H bonds in the glucopyranosyl ring are parallel or antiparallel; thus, $^1\mathscr{D}_{CH}$ (one-bond C–H RDCs) provide two independent measurements in the glucopyranosyl ring. To increase the number of independent parameters, 23 RDCs were measured for the glucopyranosyl ring and 12 for the fructofuranosyl ring (Table 1).[18] These measurements included $^2\mathscr{D}_{CH}$ and $^3\mathscr{D}_{CH}$ (two and three bond ^{13}C–^1H long-range RDCs), $^3\mathscr{D}_{HH}$ (three bond ^1H–^1H RDCs), $^1\mathscr{D}_{CC}$ and $^2\mathscr{D}_{CC}$ (one-bond and two-bond ^{13}C–^{13}C RDCs).

We began qualitatively by examining $^1\mathscr{D}_{CH}$, measured for the two rings from ^1H–^{13}C constant-time HSQC spectra.[18,45,46] $^1\mathscr{D}_{CH}$ values in the glucopyranosyl ring have the opposite sign to the corresponding values measured in the fructofuranosyl ring (Table 1). This difference in sign implies that, on average, the C–H bonds in the glucopyranosyl ring are perpendicular to C–H bonds in the fructofuranosyl ring. Thus, a cursory examination of $^1\mathscr{D}_{CH}$ can give qualitative insight into sucrose's three-dimensional structure. The relative C–H bond-orientations will later be used to aid in interpreting the range of possible structures.

RDCs are used together with a structural model, which provides the direction cosines for each internuclear vector. Alignment tensors describe the average orientation of molecules relative to the static magnetic field. Fits to RDCs yield a dipolar tensor $D(\theta, \phi)$, comprised of D_a, D_r and angles relating the bond vectors in the molecular frame to the alignment frame (Eq. 3).[43]

$$D(\theta,\phi) = D_a\left(3\cos^2\theta - 1\right) + \frac{3}{2}D_r\sin^2\theta\cos 2\phi \qquad (3)$$

In Eq. 3, D_a and D_r are the axial and rhombic components of the tensor, **D**, described by

Table 1. RDCs and scalar couplings measured in sucrose

Atom Pair	J	J'	RDC ($\mathscr{D}$)
Glucopyranosyl ring			
C-1g–H-1g	169.61 ± 0.1	177.69 ± 0.1	8.08 ± 0.2
C-2g–H-2g	143.93 ± 0.1	150.15 ± 0.1	6.22 ± 0.2
C-3g–H-3g	145.36 ± 0.1	152.79 ± 0.1	7.43 ± 0.2
C-4g–H-4g	144.79 ± 0.1	149.16 ± 0.1	4.37 ± 0.2
C-5g–H-5g	144.88 ± 0.1	150.49 ± 0.1	5.62 ± 0.2
C-2g–H-1g	−1.67 ± 0.03	−2.49 ± 0.03	−0.82 ± 0.06
C-3g–H-1g	6.15 ± 0.5	5.91 ± 0.5	0.25 ± 1.0
C-3g–H-2g	−3.26 ± 0.06	−2.31 ± 0.24	0.95 ± 0.3
C-3g–H-4g	−3.75 ± 0.7	−3.58 ± 0.76	0.17 ± 1.46
C-4g–H-2g	0.84 ± 0.4	1.43 ± 0.34	0.59 ± 0.75
C-4g–H-3g	−4.79 ± 0.5	−3.63 ± 0.34	1.15 ± 0.85
C-4g–H-5g	−4.60 ± 0.09	−5.45 ± 0.16	−0.85 ± 0.25
C-5g–H-1g	6.63 ± 0.5	6.60 ± 0.2	−0.03 ± 0.7
H-1g–H-2g	3.9 ± 0.1	1.47 ± 0.3	−2.43 ± 0.4
H-2g–H-3g	10.0 ± 0.1	12.1 ± 0.1	2.1 ± 0.2
H-3g–H-4g	9.2 ± 0.1	10.0 ± 0.1	0.8 ± 0.2
H-4g–H-5g	10.3 ± 0.1	8.5 ± 0.1	−1.8 ± 0.2
C-1g–C-2g	46.1 ± 0.1	44.4 ± 0.3	−1.7 ± 0.4
C-2g–C-3g	38.1 ± 0.1	38.8 ± 0.1	0.7 ± 0.2
C-3g–C-4g	38.1 ± 0.1	38.4 ± 0.1	−0.3 ± 0.2
C-4g–C-5g	40.1 ± 0.1	38.8 ± 0.1	−1.3 ± 0.2
C-5g–C-6g	43.2 ± 0.1	43.5 ± 0.1	0.3 ± 0.2
C-4g–C-6g	4.0 ± 0.1	3.4 ± 0.1	−0.6 ± 0.2
Fructofuranosyl ring			
C-3f–H-3f	143.1 ± 0.1	129.9 ± 0.1	−13.2 ± 0.2
C-4f–H-4f	138.4 ± 0.1	130.0 ± 0.1	−8.4 ± 0.2
C-5f–H-5f	147.1 ± 0.1	128.9 ± 0.1	−18.2 ± 0.2
C-3f–H-4f	−2.15 ± 0.03	−1.65 ± 0.02	0.5 ± 0.05
C-4f–H-3f	−3.59 ± 0.05	−2.22 ± 0.05	1.4 ± 0.1
C-5f–H-4f	−1.2 ± 0.2	−0.6 ± 0.2	0.6 ± 0.4
H-3f–H-4f	8.63 ± 0.1	8.2 ± 0.1	−0.43 ± 0.2
H-4f–H-5f	8.4 ± 0.1	5.8 ± 0.1	−2.6 ± 0.2
C-1f–C-2f	51.6 ± 0.15	52.1 ± 0.15	0.5 ± 0.3
C-2f–C-3f	43.6 ± 0.15	47.0 ± 0.15	3.4 ± 0.3
C-3f–C-4f	38.8 ± 0.15	39.9 ± 0.15	1.1 ± 0.3
C-4f–C-5f	39.9 ± 0.15	40.3 ± 0.15	0.4 ± 0.3
C-5f–C-6f	41.5 ± 0.15	41.0 ± 0.15	−0.5 ± 0.3

$1/3[D_{zz} - (D_{xx} + D_{yy})/2]$ and $1/3[D_{xx} - D_{yy}]$, respectively,[47] θ is the angle given bond vector makes with the principle axis of the tensor, and ϕ is the angle describing the position of the projection of the internuclear vector on the x–y plane relative to the x-axis. The alignment tensor is unitless; its components, A_a and A_r can be calculated from the relations:

$$A_a = \frac{D_a}{-(\mu_0 h/16\pi^3)\gamma_A\gamma_B\langle r^{-3}\rangle}, \text{ and}$$
$$A_r = \frac{D_r}{-(\mu_0 h/16\pi^3)\gamma_A\gamma_B\langle r^{-3}\rangle} \quad (4)$$

where μ_0 is the permittivity of a vacuum, h is Planck's constant, γ_A and γ_B are the magnetogyric ratios of nuclei A and B respectively, and r is the A–B internuclear distance.

We calculated the alignment tensor for the glucose ring, assuming that it is rigid. To fit the isolated glucose ring, we extracted its coordinates from the neutron structure and fit RDCs measured for this ring. RDCs measured for the glucopyranosyl ring fit well (Fig. 3) to the structure, as expected for a rigid fragment. Some of the outliers are likely results of inaccuracies in structure, experimentally determined RDCs or molecular vibrations unaccounted for by static structures.[48] Both rings fit well to the RDCs having reasonable χ^2 and Q values.[49] Table 2 lists the values of the alignment tensors for each of the fructofuranosyl ring puckers for comparison with the glucopyranosyl ring. It has been demonstrated that when the coordinates of a rigid molecule

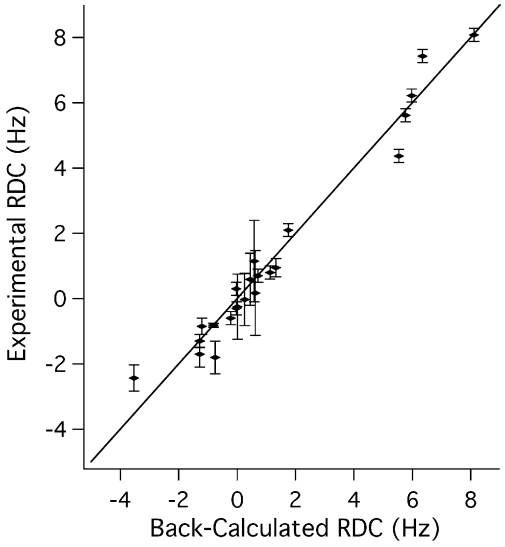

Figure 3. A scatter plot of measured RDCs versus back-calculated RDCs for the glucopyranosyl ring ($R = 0.983$). The line at $x = y$ is plotted as a guide to evaluate deviation from ideal correlation.

Table 2. Alignment tensors and fitting results for the individual rings in sucrose

Fragment or Pucker form	$D_a \times 10^{-4}$	$D_r \times 10^{-4}$	Q factor (R)[49]	χ^2
Glucopyranosyl	**−1.58 ± 0.07**	**−0.39 ± 0.11**	**0.17 (0.983)**	**78.6**
Fructofuranosyl (0)	4.58 ± 0.27	1.35 ± 0.12	0.08 (0.994)	77.2
Fructofuranosyl (18)	4.27 ± 0.25	0.99 ± 0.13	0.08 (0.996)	57.2
Fructofuranosyl (36)	3.82 ± 0.23	0.08 ± 0.23	0.07 (0.998)	38.2
Fructofuranosyl (54)	3.42 ± 0.20	0.79 ± 0.04	0.07 (0.999)	30.1
Fructofuranosyl (72)	3.42 ± 0.15	1.10 ± 0.09	0.07 (0.998)	40.1

are divided into smaller fragments, the alignment tensor remains the same for each fragment as for the intact molecule.[20,50] D_a for the glucopyranosyl ring is two to threefold less than the corresponding values for the fructofuranosyl ring.[38] Mirroring the relative signs of the ${}^1\mathscr{D}_{CH}$ values, D_a values for glucopyranosyl have the opposite sign from those in the fructofuranosyl ring. The errors in each fit[39] demonstrate that values of the best fit alignment tensors for each of the two rings are significantly different, and are not within experimental error. This result indicates internal motion in sucrose.

Having established the existence of internal motion in sucrose, we focus on whether the averaged RDCs in each ring are a result of motional averaging within a single conformational well or among multiple conformational wells. To answer this question, we fit RDCs to each rigid structure for each of the four force fields and determined the best fit by finding the region(s) with the lowest χ^2. Motional averaging within a single potential energy well would yield one minimum for ϕ and ψ, or a range of good fits in the same ϕ, ψ vicinity. Conversely, if jumps between conformational wells are occurring, fits would likely show that more than one region is populated, and the χ^2 of the best-fit regions should be greater than the sum of the individual rings' χ^2.

Contour plots of RDC fits to the force-field specific structures (Fig. 4) show four regions of acceptable fits, all of which are found in the range $0° \leqslant \phi \leqslant 180°$. In contrast to fits of RDCs to structures with unrestrained puckers, those with restrained puckers are more consistent across force fields. Here we abbreviate these ϕ, ψ regions as: D1 = (120°, 270°); D2 = (45°, 300°); D3 = (90°, 180°); D4 = (90°, 120°), where the coordinates listed are the approximate centers of the respective regions. Note that more than one region of ϕ, ψ space is populated, and the region corresponding to D1 on the ϕ, ψ map coincides with the X-ray structure. The regions all have similar χ^2 values, and dominant conformers are not distinguishable based on this criterion alone. Figure 4 illustrates that the best-fit regions depend on pucker phase, and the consequence of not restraining the phase. This result not only highlights the sensitivity of RDCs to fructofuranosyl pucker, but to overall structural differences as well. Nevertheless, D1 and D2 are the two dominant forms, remaining well fit across various puckers and force field generated structures. The primary force-field variations are the broad, shallow minimum suggested by merger of D1 and D2 for the Accelrys force field, compared to two local minima suggested by CSFF and CHARMM22, and the substantially higher χ^2 values observed for structures generated with the Homans force field. Another force-field variation we observe is that structures having identical ϕ, ψ values, yield dissimilar χ^2 values. Since the input RDCs are identical, this result demonstrates that

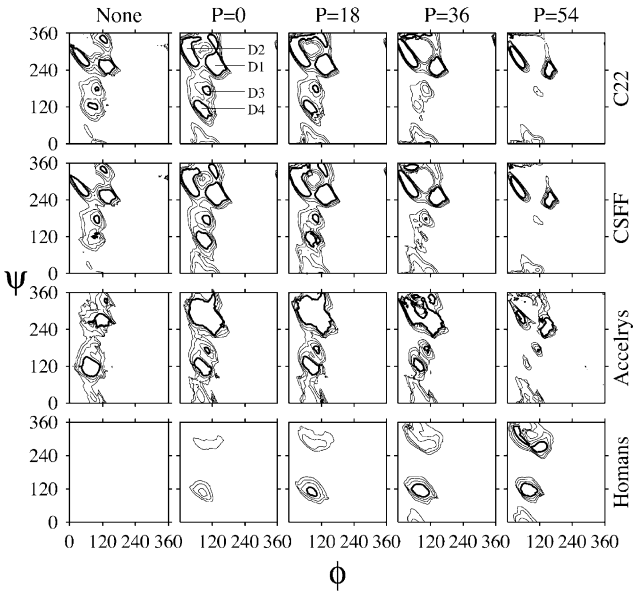

Figure 4. RDC fitting maps as a function of force field. The leftmost column are fits to the structures calculated with unrestrained fructose puckers. The remaining four columns were fit to structures with restrained fructofuranosyl puckers indicated at the top of the column. The structures were calculated by CHARMM22, CSFF, Accelrys, and Homans force fields indicated on the right. The bold contours show the $\chi^2 = 600$ cutoff used in comparisons of the fits to the potential energy surfaces calculated by force fields (Fig. 6); the thin outer contours are at $\chi^2 = 700$, 800, and 900. The general regions where χ^2 minima were found are labeled as D1–D4 on the second panel of the top row.

each force field yields slightly different structures for the same ϕ, ψ values. Finally, we observe that the lowest χ^2 value is threefold higher than the sum of the χ^2 values for individual rings. This poor fit establishes that no one structure fits well to the RDCs. Altogether, the results of these fits suggest jumping between multiple potential energy wells in sucrose.

3.3. Comparison of RDC fits and force-field energy maps

The results of RDC fits may be virtual structures due to motional averaging. To explore this possibility, we compare the RDC fits with force-field results. The reasonable agreement between RDC fits and force-field (Fig. 5A) energy maps can be improved if the results of the RDCs fit to structures generated with the Accelrys force field are superposed on CSFF PES maps (Fig. 5B). Both sets of maps suggest that D1/M1, D2/M2, and D3/M3 are dominant conformations in sucrose, and allow for some sampling of M4 (note that D4 and M4 do not coincide). The force fields and RDC fits disagree regarding the importance of D4. While structures in this region have low χ^2 values when fit to RDCs, all but the Homans force field suggest D4 is unpopulated. To reconcile this discrepancy, we use the relative orientations of the axial C–H bonds in the two rings. As stated earlier, the C–H bonds in the glucose ring are roughly perpen-

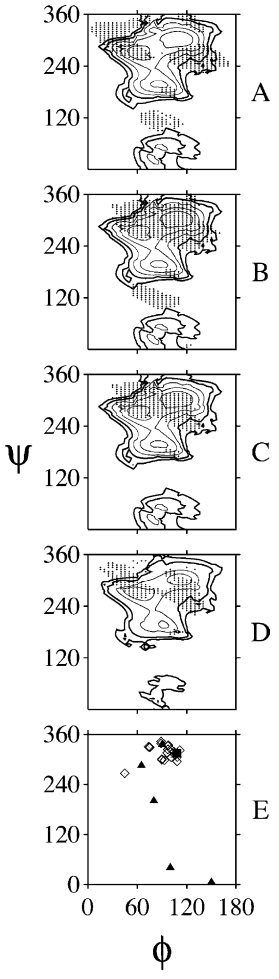

Figure 5. Plots displaying χ^2 minima from RDC fits (points) overlaid on potential energy surfaces (contour lines) as a function of force field. (A) RDC fits to CSFF generated structures with a pucker phase of 18° (points), overlaid on the PES calculated by CSFF. (B) RDC fits to Accelrys generated structures with a pucker phase of 18° (dots), overlaid on the PES calculated by CSFF. (C) Same as panel B, but with angular constraints of 90 ± 30°. This panel shows that imposing angular constraints results in elimination of D4. (D) Same as panel C, except that the calculations are for fructofuranosyl ring pucker phase of 36°. This panel shows the sensitivity of the RDC fits and the PES on pucker phase. (E) A ϕ, ψ map displaying the glycosidic torsions from sucrose's neutron crystal structure (square),[2] the NMR solution structures by Pérez and co-workers (triangles),[13] and structures of sucrose bound to proteins (diamonds; see Table 3).

dicular to those in the fructose ring based on the relative signs of their $^1\mathscr{D}_{CH}$. We reduced the range of acceptable structures by examining the angle between C–H bond vectors in the two rings in the calculated structures. We reasoned that the orientation of the C–H bonds in the two rings could be accounted for by constraining acceptable RDC fits to those where the inter-ring angles between the C–H bond vectors have values between 60° and 120° (90° ± 30°). RDC maps filtered by these angle constraints were superimposed on the force-field energy maps. This approach results in improved agreement between RDCs and force fields (Fig. 5C). These results suggest that the dominant ϕ, ψ values for sucrose are in D1/M1 and D2/M2, with a minor contribution from D3/M3, and perhaps M4. Since D4 was excluded in the ϕ, ψ space mapped out by the angular constraints and conflicts with the force-field maps this region is unlikely.

3.4. Fits of multiple conformations to one set of RDCs

To further test our hypothesis of the existence of multiple conformations, we fitted two conformers to the RDCs. Using computer subroutines available in NMRPipe[39] we fitted all possible two-structure combinations using structures from calculated minima M1, M2, M3, and M4. Because CSFF and C22 yielded similar fits (see later), we used CSFF generated structures in the multiple conformer analysis to represent both force fields. We also fitted two-structure combinations using minima found by the Accelrys force field because it is provided with widely used commercial software.

Some of the combinations calculated using this fitting strategy yielded χ^2 values nearly threefold lower than any of the single structure fits, resulting in significantly better agreement between experimental and back-calculated RDCs. This is emphasized in Figure 6 for M2 and M4 using CSFF generated structures and M2 and M3 using Accelrys generated structures. Improved agreement is seen for CSFF generated structures when the pairs from minima M1 and M2, M1 and M3, M2 and M3, and M2 and M4, for fructose puckers of 18° and 36°. Similarly, agreement is improved for Accelrys generated structures when the pairs from minima M1 and M2, M2, and M3, and M2 and M4, for fructose puckers of 18° and 36°. The improved fits for two structures support motional averaging among the calculated minimum energy wells, M1, M2, M3, and M4 in sucrose, but the two force fields tested give an inconsistent picture. Similar to the single structure fits, the results of two-structure fits are force field dependent. There is also no clear convergence toward two dominant structures, one of which is in the M1 crystal well, as one might expect. Nevertheless, two or more conformations are indicated here by virtue of the reduction in χ^2.

Because the number of independent RDCs is restrictive, we did not attempt simultaneous fits of more than two conformers. Each conformer requires five independent RDCs, and fitting three or more structures to the RDCs requires at least 15 independent RDCs. With the limited number of independent RDCs, we chose to leave the problem overdetermined with two structure fits.

4. Discussion

The data presented establish that sucrose interconverts among multiple conformations representing separate

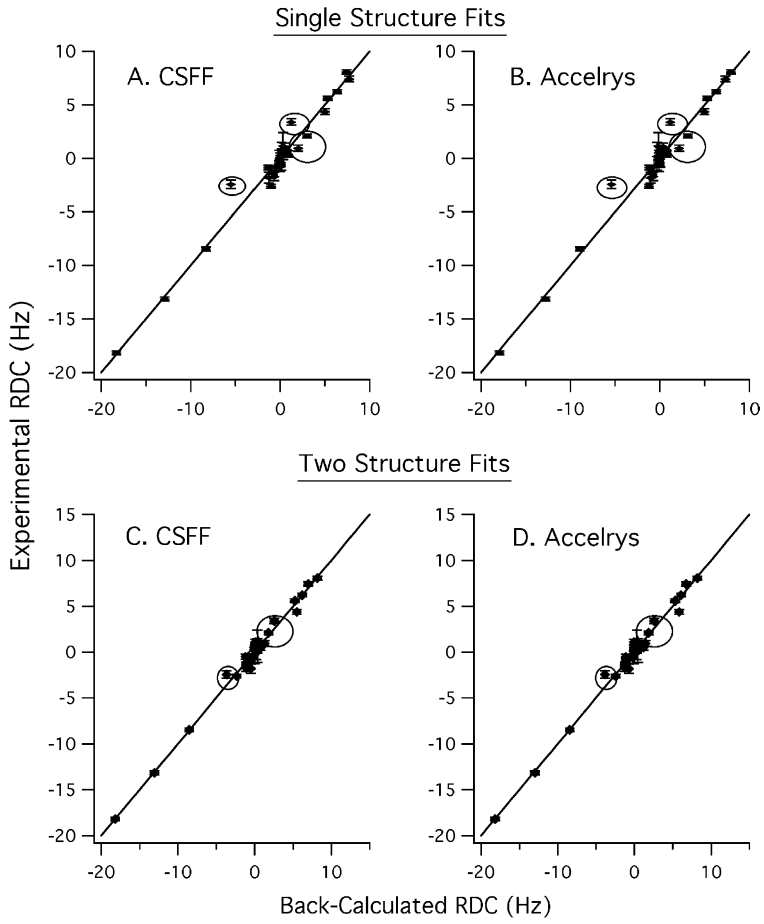

Figure 6. Scatter plots showing the best fit of RDCs to single structure models from CSFF (panel A) and Accelrys (panel B). The best fit single structures are from the M1 region have ϕ, ψ values of (125°, 260°) and (130°, 270°). Plots in panels C (CSFF) and D (Accelrys) show the improvement in back-calculated RDCs when two structures are fit to the RDCs. The best fit two-structure models for CSFF are from M2 and M4 with a pucker phase of 36°; best fit two-structure models for Accelrys are from M2 and M3 with a pucker phase of 36°.

energy wells. This outcome is based on a difference in D_a and D_r obtained from liquid-crystalline media, poor fits of single structures to the experimental RDCs, and decreases in χ^2 values for simultaneous fits of two structural models to the same RDCs. Note that the two-structure fits were only reported for minima calculated by CSFF and Accelrys and that no virtual structures were included in these fits. The present report contains data measured in one liquid-crystalline medium, though structural studies of other molecules have utilized more than one liquid crystalline medium to deduce structure. Multiple media are particularly suited to deducing relative orientations of two fragments in fairly rigid molecules. A second alignment medium usually does not provide additional structural information in the case of flexible molecules. We and others demonstrated that motion can be deduced from measurements in a single alignment medium.[18,20,24] In the present case, the force field calculations and the results of previous studies are more helpful than a second alignment medium. Thus, the RDC fits and force-field calculations reported herein demonstrate that D1/M1, D2/M2, D3/M3, and M4 are the most probable individual conformations contributing to sucrose's averaged structure in solution.

Multiple wells indicate internal motion in sucrose. In the limit of fast motion, NMR data is the average of independent conformations, thus, the conformations cannot be deduced from NMR measurements alone. Delineation of structure and dynamics would be facilitated by knowledge of independent conformations, which in principle, can be accomplished with the aid of force fields. However, using force fields to aid in interpretation of sucrose RDC fitting results can depend on the selected force field, as demonstrated in the single structure fits. For example, one might conclude that sucrose is confined to M1 and M2 with conformational jumping to M3 from the recently developed CSFF force field, whereas the broader minima of the Homans force field leads one to conclude that M1, M2, and M3 are more easily and equally sampled by sucrose (Fig. 2).

The benefit of using multiple force fields to interpret carbohydrate structures is an important result of this study, especially given the status of carbohydrate force field development compared to force fields for proteins

and nucleic acids. The comparison of RDC fits and PES from each force field led directly to our appreciation of the importance of the fructofuranosyl pucker phase in calculating the structures and energies of sucrose. It is encouraging that all the molecular mechanics force fields tested here (Fig. 2) and RDCs (Fig. 4) independently show that $60° \leqslant \phi \leqslant 180°$. Low probability of finding $\phi > 180$ is likely a consequence of unfavorable steric clashes between glucopyranosyl ring OHs and the fructofuranosyl anomeric CH_2OH group.

Inconsistency in the details in ψ was observed across force fields tested here. Consequently, these features required deeper examination. The inconsistency in ψ also highlights a possible problem, namely using force fields to interpret fits to RDC data can yield force-field dependent results. As shown above, RDC fits to Accelrys generated structures resulted in surfaces, which are in best agreement with the PES calculated from CSFF. When overlaid on these surfaces, the RDC fits indicate that D1/M1, D2/M2 and D3/M3 are the likeliest molecular conformations.

Though it is not as strongly indicated by RDC fits, force fields suggest that M4 ($\phi, \psi = 90°, 60°$) is populated. This region has similar ϕ values to D4, but the ψ values calculated by force fields are lower. It is possible that acceptable fits in the D4 region represent virtual structures of stable conformations from M4 and D1/M1, D2/M2, or D3/M3. It is also possible that the M4 conformations are present in small amounts. If this were the case, it would be difficult to detect these conformations by RDCs from NMR spectra in the fast-exchange regime. The observed RDCs would be a weighted average, influenced by the small populations, resulting in structures with unphysical ϕ, ψ coordinates. Similarly, motion may influence the outcome of two-structure fits. Fits of more than two structures are technically feasible, but this possibility could not be reliably tested because there were insufficient independent RDC measurements. Other pairings of structures are also possible as a result of a correlation between pucker phase and glycosidic torsions, ϕ and ψ. This is suggested by the force-field maps (Fig. 2), which were calculated as a function of pucker phase. Since fructose pucker interconversion occurs rapidly, this type of analysis is precluded by the difficulty of detecting the individual pucker forms.

In their study, Pérez and co-workers concluded that the potential energy maps from force-field calculations overlaid on NOE maps suggest that sucrose is interconverting rapidly, but that the motion is limited.[13] They identified five conformations for sucrose (shown in Fig. 5 as triangles), three corresponding to D1/M1, D2/M2, and D3/M3, and the other two corresponding to M4.

Results of a recent study by French et al., who use a combination of quantum mechanics and the MM3 force field to map the PES of sucrose,[51] compare favorably with the results from the present study. Their results suggest that there are two major forms of sucrose corresponding to D1/M1 and D2/M2 in the present study, and two higher energy local minima, which correspond to D3/M3 and M4 in the present study. D1/M1 and D2/M2 are separated by a low-energy barrier (~3 kcal/mol) in French et al.'s study, which indicates discrete states and motion. D1/M1 and M4 are separated by a slightly higher barrier as are D2/M2 and D3/M3. The low barriers separating the local minima support facile interconversion among the states.

Flexibility in sucrose is also indicated in a solid-state NMR report.[14] Grant and co-workers examine the chemical shift tensors of single crystals of sucrose and compare them to isotropic chemical shifts obtained from magic angle spinning experiments and to solution data. The isotropic shifts in the solid state do not match those obtained in solution. This finding demonstrates that the while sucrose exists in a single conformation in the crystalline state, it is flexible in solution.

Flexibility in sucrose may play an important role in biological function. Table 3 lists ϕ and ψ values for free sucrose and sucrose bound to various proteins or

Table 3. ϕ and ψ values for sucrose bound to proteins or enzymes

Structure (pdb name)	ϕ (deg)	ψ (deg)	Enzyme type/family	Protein Data Bank Filename
Crystal structure[6]	108	−45		SUCROS04[66]
Amylosucrase sucrose complex[53]	44	−93	Hydrolase	1JGI.pdb
Amylosucrase sucrose complex[52]	89	−22	Glucosyl transferase	1MW1.pdb
Fructosyl transferase sucrose complex[61]	111	−38	Fructosyl transferase	1PT2.pdb
β-Glucosidase sucrose complex[67]	89	−17	β-Glucosidase	1GNX.pdb
GDP mannose dehydrogenase–sucrose complex[62]	104	−42	Glucose-specific dehydrogenase	1MV8.pdb
	109	−54		
ScrY (2 bound sucrose molecules)[4]	75	−31	Sucrose-specific porin	1A0T.pdb
	90	−61		
Maf from *Bacillus subtillis*–sucrose complex[63]	101	−36	Unknown	1EX2.pdb
Pterocarpus lectin[64]	118	−47	Lectin	1N3P.pdb
Pea lectin (2 bound sucrose molecules)[67]	96	−44	Lectin	1OFS.pdb
	101	−55		
Lentil lectin–sucrose complex[65]	107	−58	Lectin	1LES.pdb

enzymes. Proteins listed in the table fall into three categories: (1) enzymes which act directly on sucrose, such as amylosucrase,[52] (2) enzymes where sucrose is bound in place of the natural substrate; (3) and proteins which do not act enzymatically on sucrose, but are responsible for transporting the disaccharide. Amylosucrase is responsible for cleaving the glucopyranosyl–fructofuranosyl bond and building glycogen chains. In the case of glucose hydrolysis, it is important for the glucopyranosyl ring oxygen atom lone pair to be antiperiplanar to the glycosidic oxygen to facilitate the leaving of the fructofuranosyl ring.[52] In this structure, the disaccharide conformation is in agreement with D2/M2 (Fig. 5E), while the commonly reported structure is in M1/D1.[53] Proteins such as the sucrose-specific porins, are responsible for transporting sucrose in and out of cells.[54] In these cases the conformation of bound sucrose may not be as crucial as in the amylases, but sucrose must still bind specifically. Many of the bound sucrose structures have ϕ, ψ values in the D1/M1 region. Thus, it appears that sucrose must be flexible in order to bind its target proteins, although crystal conformations in the M3 or M4 region are not observed in the structures surveyed.

The conclusions detailed above stand in direct contrast to those of a number of previous studies, which state that sucrose is rigid.[7–9] Some of these studies attempted to detect motion through nuclear relaxation. Another uses a combination of NOEs, RDCs, and J couplings in X-plor to probe sucrose structure.[7] ^{13}C T_1s are sensitive to motion that is faster than the overall correlation time of the molecule (ca. 90 ps at about 315 °C).[13] The relaxation study reports ^{13}C nuclear relaxation measured at −30 °C in a mixture of D_2O–Me_2SO. But even at low temperatures where the correlation time is increased, ^{13}C T_1s may not be sufficiently sensitive to detect internal motion if this motion takes place on a slower timescale than overall tumbling.[55–57] Furthermore, the presence of Me_2SO may influence the equilibrium conformation of sucrose in different ways than the D_2O buffer used in the present study. Thus, it is difficult to directly compare their results obtained in a mixed solvent system with those obtained in this study (20 mM Na_2PO_4/D_2O at 42 °C). A recent report used X-plor in conjunction with the Homans potential to conclude that the solution structure of sucrose is similar to that of the crystal structure, but detected no other conformations.[7] For minor structures to be detected, the program may need stronger restraints, a larger number of input RDCs, NOEs, or J values. In addition, as we found in this study, the Homans-based force field may not properly describe the PES of sucrose; fructose and other furanoses were neither included in the target data, nor were any tests on furanose rings included in the original published force field.

Despite the fact that ^{13}C relaxation data[8,9] and some solution-state structural studies[5,7] imply rigidity in sucrose, disagreement with the results of the present study is superficial and can be resolved. When the lifetime of the individual conformations is on the timescale of tens or hundreds of nanoseconds the motion interconverting them cannot be detected in relaxation measurements. In contrast to nuclear relaxation, RDCs are modulated by all motion, from small vibrations, to overall molecular tumbling, to conformational motion affecting all atoms in the molecule, and the lifetimes of the conformational states. Thus, RDCs can complement nuclear relaxation, and motion undetected from nuclear relaxation measurements can be detected with RDCs. Alternatively, the short overall molecular correlation time for sucrose (90 ps at 315 K)[31] in water ensures that nuclear relaxation occurs mainly as a result of overall molecular reorientation, hence any motion taking place slower than the correlation time of the molecule, but faster than microsecond, will not lead to observable relaxation.[55,58] In this way, the molecule may appear rigid even when significant motion is ongoing.

5. Conclusions

We have shown from a combination of RDC measurements and four force fields that multiple conformations are present and motion is ongoing for sucrose in aqueous solution. Single structure fits indicate likely conformations of sucrose, which generally agree with force-field generated PESs. Furthermore, the improved fits to two structures demonstrate that sucrose interconverts between at least two conformations.

RDC and force-field results reported herein suggest that while CSFF may have reasonable parameters for the glycosidic torsions, parameters for the individual residues are not optimal. The opposite is true for the Accelrys force field; the glycosidic parameters may not be optimal, but those for the glucose and fructose rings may be more realistic than the other force fields tested here. The current situation may be more complex due to several motions on multiple timescales: pucker changes may be rapid, which could modulate RDCs but not ^{13}C T_1s. At the same time, jumps resulting in conformational changes from motion about the glycosidic torsions occur at a frequency that does not affect nuclear relaxation measurements.

These results do not conflict with studies suggesting that sucrose is rigid. The apparent discrepancy is alleviated by considering that ^{13}C relaxation is sensitive to motions faster than the overall molecular correlation time (~90 ps at 315 K), even at cryogenic temperatures. While nuclear relaxation measurements are useful in deducing motion, which occurs faster than overall molecular tumbling, motion on the tens of nanoseconds to microseconds timescale may go undetected in ^{13}C relaxation experiments. RDCs are sensitive to this

motion, and this demonstrates how they can be used to detect motion beyond the limits of ^{13}C relaxation. The present results demonstrate that a molecule can be dynamic and yet appear rigid if only certain measurements are made. Similar conclusions were reported previously by Widmalm and co-workers.[59] The flexibility in sucrose appears to be important for binding to target enzymes in hydrolysis and synthesis of glycogen.

Acknowledgements

We gratefully acknowledge Richard Pastor and Dennis Torchia for helpful discussions and Dan Garrett for PIPP.[60]

References

1. Skov, L. K.; Mirza, O.; Henriksen, A.; Potocki De Montalk, G.; Remaud-Simeon, M.; Sarçabal, P.; Willemot, R.-M.; Monsan, P.; Gajhede, M. *J. Biol. Chem.* **2001**, *276*, 25273–25278.
2. Skov, L. K.; Mirza, O.; Sprogoe, D.; Dar, I.; Remaud-Simeon, M.; Albenne, C.; Monsan, P.; Gajhede, M. *J. Biol. Chem.* **2002**, *277*, 47741–47747.
3. Hamada, S.; Slade, H. D. *Microbiol. Rev.* **1980**, *44*, 331–384.
4. Forst, D.; Welte, W.; Wacker, T.; Diederichs, K. *Nat. Struct. Biol.* **1998**, *5*, 37–46.
5. Bock, K.; Lemieux, R. U. *Carbohydr. Res.* **1982**, *100*, 63–74.
6. Brown, G. M.; Levy, H. A. *Acta Crystallogr., Sect. B* **1973**, *29*, 790–797.
7. Neubauer, H.; Meiler, J.; Peti, W.; Griesinger, C. *Helv. Chim. Acta* **2001**, *84*, 243–258.
8. Kovacs, H.; Bagley, S.; Kowalewski, J. *J. Magn. Resonance* **1989**, *85*, 530–541.
9. Effemey, M.; Lang, J.; Kowalewski, J. *Magn. Resonance Chem.* **2000**, *38*, 1012–1018.
10. Batta, G.; Kover, K. E. *Carbohydr. Res.* **1999**, *320*, 267–272.
11. Adams, B.; Lerner, L. *J. Am. Chem. Soc.* **1992**, *114*, 4827–4829.
12. Poppe, L.; van Halbeek, H. *J. Am. Chem. Soc.* **1992**, *114*, 1092–1094.
13. Hervé du Penhoat, C.; Imberty, A.; Roques, N.; Michon, V.; Mentech, J.; Descotes, G.; Pérez, S. *J. Am. Chem. Soc.* **1991**, *113*, 3720–3727.
14. Sherwood, M. H.; Alderman, D. W.; Grant, D. M. *J. Magn. Resonance, Ser. A* **1993**, *104*, 132–145.
15. Stevens, E. S.; Duda, C. A. *J. Am. Chem. Soc.* **1991**, *113*, 8622–8627.
16. Duda, C. A.; Stevens, E. S. *Carbohydr. Res.* **1990**, *206*, 347–351.
17. Duker, J. M.; Serianni, A. S. *Carbohydr. Res.* **1993**, *249*, 281–303.
18. Freedberg, D. I. *J. Am. Chem. Soc.* **2002**, *124*, 2358–2362.
19. Rundlöf, T.; Landersjö, C.; Lycknert, K.; Maliniak, A.; Widmalm, G. *Magn. Resonance Chem.* **1998**, 773–776.
20. Tian, F.; Al-Hashimi, H. M.; Craighead, J. L.; Prestegard, J. H. *J. Am. Chem. Soc.* **2001**, *123*, 485–492.
21. Manuel-Pastor, M.; Bush, C. A. *Carbohydr. Res.* **1999**, *323*, 147–155.
22. Kiddle, G. R.; Homans, S. W. *FEBS Lett.* **1998**, *436*, 128–130.
23. Tjandra, N.; Bax, A. *Science* **1997**, *278*, 1111–1114.
24. Tolman, J. R.; Al-Hashimi, H. M.; Kay, L. E.; Prestegard, J. H. *J. Am. Chem. Soc.* **2001**, *123*, 1416–1424.
25. Tolman, J. R.; Flanagan, J. M.; Kennedy, M. A.; Prestegard, J. H. *Proc. Natl. Acad. Sci. U.S.A.* **1995**, *92*, 9279–9283.
26. Saupe, A. *Angew. Chem., Int. Ed. Engl.* **1968**, *7*, 97–112.
27. Tolman, J. R.; Flanagan, J. M.; Kennedy, M. A.; Prestegard, J. H. *Nat. Struct. Biol.* **1997**, *4*, 292–297.
28. Howard, K. P.; Opella, S. J. *J. Magn. Resonance, Ser B.* **1996**, *112*, 91–94.
29. Ottiger, M.; Bax, A. *J. Biomol. NMR* **1998**, *12*, 361–372.
30. Zhu, G.; Renwick, A.; Bax, A. *J. Magn. Resonance, Ser. A* **1994**, *110*, 257–261.
31. Rundlöf, T.; Venable, R. M.; Pastor, R. W.; Kowalewski, J.; Widmalm, G. *J. Am. Chem. Soc.* **1999**, *121*, 11847–11854.
32. Bible, R. H. *Interpretation of NMR Spectra*; Plenum: New York, 1965.
33. Hoye, T. R.; Hanson, P. R.; Vyvyan, J. R. *J. Org. Chem.* **1994**, *59*, 4096–4103.
34. Delaglio, F.; Wu, Z.; Bax, A. *J. Magn. Resonance* **2001**, *149*, 276–281.
35. Altona, C.; Sundaralingam, M. *J. Am. Chem. Soc.* **1972**, *94*, 8205–8212.
36. Brooks, B. R.; Bruccoleri, R. E.; Olafson, B. D.; States, D. J.; Swaminathan, S.; Karplus, M. *J. Comput. Chem.* **1983**, *4*, 187–217.
37. Momany, F. A.; Rone, R. *J. Comput. Chem.* **1992**, *13*, 888–900.
38. Losonczi, J. A.; Andrec, M.; Fischer, M. W. F.; Prestegard, J. H. *J. Magn. Resonance* **1999**, *138*, 334–342.
39. Delaglio, F.; Grzesiek, S.; Vuister, G.; Zhu, G.; Pfeifer, J.; Bax, A. *J. Biomol. NMR* **1995**, *6*, 277–293.
40. Ha, S. N.; Giammona, A.; Field, M.; Brady, J. W. *Carbohydr. Res.* **1988**, *180*, 207–221.
41. Kuttel, M.; Brady, J. W.; Naidoo, K. J. *J. Comput. Chem.* **2002**, *23*, 1236–1243.
42. Homans, S. W. *Biochemistry* **1990**, *19990*, 9110–9118.
43. Bax, A.; Kontaxis, G.; Tjandra, N. In *Dipolar Couplings in Macromolecular Structure Determination*; James, T. L., Dotsch, V., Schmitz, U., Eds.; Academic: San Diego, 2001; 339 Part B, pp 127–174.
44. Meiler, J.; Blomberg, N.; Nilges, M.; Griesinger, C. *J. Biomol. NMR* **2000**, *16*, 245–252.
45. Bodenhausen, G.; Ruben, D. J. *Chem. Phys. Lett.* **1980**, *69*, 185–189.
46. Vuister, G.; Bax, A. *J. Magn. Resonance* **1992**, *98*, 428–435.
47. Clore, G. M.; Gronenborn, A. M.; Bax, A. *J. Magn. Resonance* **1998**, *133*, 216–221.
48. Negin, R. S.; Woodcock, L.; Venable, R.; Freedberg, D. I., in preparation.
49. Cornilescu, G.; Marquardt, J. L.; Ottiger, M.; Bax, A. *J. Am. Chem. Soc.* **1998**, *120*, 6836–6837.
50. Fischer, M. W. F.; Losonczi, J. A.; Weaver, J. L.; Prestegard, J. H. *Biochemistry* **1999**, *38*, 9013–9022.
51. French, A. D.; Kelterer, A.-M.; Cramer, C. J.; Johnson, G. P.; Dowd, M. K. *Carbohydr. Res.* **2000**, *326*, 305–322.

52. Skov, L. K.; Mirza, O.; Sprogøe, D.; Dar, I.; Remaud-Simeon, M.; Albenne, C.; Monsan, P.; Gajhede, M. *J. Biol. Chem.* **2002**, *277*, 47741–47747.
53. Mirza, O.; Skov, L. K.; Remaud-Simeon, M.; Potocki De Montalk, G.; Albenne, C.; Monsan, P.; Gajhede, M. *Biochemistry* **2001**, *40*, 9032–9039.
54. Wang, Y.-F.; Dutzler, R.; Rizkallah, P. J.; Rosenbusch, J. P.; Schirmer, T. *J. Mol. Biol.* **1997**, *272*, 56–63.
55. McCain, D. C.; Markley, J. L. *J. Am. Chem. Soc.* **1986**, *108*, 4259–4264.
56. McCain, D. C.; Markley, J. L. *Carbohydr. Res.* **1986**, *152*, 73–80.
57. McCain, D. C.; Markley, J. L. *J. Magn. Resonance* **1987**, *73*, 244–251.
58. Lipari, G.; Szabo, A. *J. Am. Chem. Soc.* **1982**, *104*, 4546–4559.
59. Höög, C.; Landersjö, C.; Widmalm, G. *Chem. Eur. J.* **2001**, *7*, 3069–3077.
60. Garrett, D. S.; Powers, R.; Gronenborn, A. M.; Clore, G. M. *J. Magn. Resonance* **1991**, *95*, 214–220.
61. Meng, G.; Futterer, K. *Nat. Struct. Biol.* **2003**, *10*, 935.
62. Snook, C. F.; Tipton, P. A.; Beamer, L. J. *Biochemistry* **2003**, *42*, 4658–4668.
63. Minasov, G.; Teplova, M.; Stewart, G. C.; Koonin, E. V.; Anderson, W. F.; Egli, M. *Proc. Natl. Acad. Sci. U.S.A.* **2000**, *97*, 6328–6333.
64. Loris, R.; Imberty, A.; Beeckmans, S.; Van Driessche, E.; Read, J. S.; Bouckaert, J.; De Greve, H.; Buts, L.; Wyns, L. *J. Biol. Chem.* **2003**, *2778*, 16297–16303.
65. Casset, F.; Hamelryck, T.; Loris, R.; Brisson, J.-R.; Teillier, C.; Dao-Thi, M.-H.; Wyns, L.; Poortmans, F.; Perez, S.; Imberty, A. *J. Biol. Chem.* **1995**, *270*, 25619–25628.
66. Allen, F. H. *Acta Crystallogr.* **2005**, *B58*, 380–388.
67. Berman, H. M.; Westbrook, J.; Feng, Z.; Gilliland, G.; Bhat, T. N.; Weissig, H.; Shindyalov, I. N.; Bourne, P. E. *Nucleic Acids Res.* **2000**, *28*, 235–242.